

Photoelasticity of sodium silicate glass from first principles

D. Donadio*, M. Bernasconi

Dipartimento di Scienza dei Materiali and Istituto Nazionale per la Fisica della Materia, Università di Milano-Bicocca, Via Cozzi 53, I-20125, Milano, Italy

F. Tassone

Pirelli Cavi e Sistemi Telecom S.p.a., Viale Sarca 222, I-20126, Milano, Italy

Based on density-functional perturbation theory we have computed the photoelastic tensor of a model of sodium silicate glass of composition $(\text{Na}_2\text{O})_{0.25}(\text{SiO}_2)_{0.75}$ (NS3). The model (containing 84 atoms) is obtained by quenching from the melt in combined classical and Car-Parrinello molecular dynamics simulations. The calculated photoelastic coefficients are in good agreement with experimental data. In particular, the calculation reproduces quantitatively the decrease of the photoelastic response induced by the insertion of Na, as measured experimentally. The extension to NS3 of a phenomenological model developed in a previous work for pure a-SiO₂ indicates that the modulation upon strain of other structural parameters besides the SiOSi angles must be invoked to explain the change in the photoelastic response induced by Na.

I. INTRODUCTION

Photoelasticity is of interest from the fundamental point of view as well as for several technological applications in optics and microelectronics. For instance, photoelasticity in a-SiO₂ is known to cause a reduction of fiber Bragg gratings efficiency¹ and to produce a loss of resolution of pure silica lenses used in photolithography². Moreover, photoelasticity is directly related to the Rayleigh scattering coefficient in single-component glasses through the Landau-Placzek relation, and is thus one of the main contributions to loss in state-of-the-art silica fibers for telecommunications³. A systematic experimental study of photoelasticity in pure and modified silica glass has been reported by Schroeder in the early 80s.⁴ Brillouin scattering measurements have shown that the modification of silica glass with alkali or alkali-earth ions (Li, Na, K, Ca, and Mg) reduces sizably the photoelastic coefficients.⁴ This result is in contrast with the prediction of simple models (Lorenz-Lorentz) based on the observed increase in density and refractive index with the modifier concentration. As expected, a related reduction of the Rayleigh scattering coefficient was later measured for these glasses,³ and Lines thus suggested their use as ultra-low loss glasses for telecommunication applications.⁵

In a recent work⁶ we have shown that the photoelastic coefficients of crystalline and amorphous pure SiO₂ can be computed with good accuracy within density functional perturbation theory. A phenomenological model based on ab-initio data allowed us to identify the microscopic parameters which rule photoelasticity in pure a-SiO₂. In the present paper we have applied the same ab-initio framework to compute the photoelastic tensor of a sodium silicate glass with composition $(\text{Na}_2\text{O})_{0.25}(\text{SiO}_2)_{0.75}$ (NS3) aiming at identifying which modification either structural or electronic induced by the insertion of sodium is mostly responsible for the change in photoelastic response. Models of NS3 glass containing 84 atoms have been generated by quenching from the melt in combined classical and Car-Parrinello molecular dynamics simulations. The calculated photoelastic coefficients are in good agreement with experimental data. In particular, the calculation reproduces quantitatively the changes of the photoelastic response induced by the insertion of Na, as measured experimentally. In order to identify the microscopic mechanisms responsible for the change of the photoelastic response induced by Na, we extended to NS3 the phenomenological model developed for pure a-SiO₂ in ref.⁶. The paper is organized as follows. In section II we describe our computational framework. In section III we report the details of the structural and elastic properties of our model of NS3. The results on the calculated photoelastic tensor and their interpretation in terms of a phenomenological model are presented in sections IV and V, respectively. Section VI is devoted to discussion and conclusions.

II. COMPUTATIONAL DETAILS

A model of sodium silicate glass of composition $(\text{Na}_2\text{O})_{0.25}(\text{SiO}_2)_{0.75}$ (NS3) has been generated within a combined classical and ab-initio framework which has been previously used to generate models of pure a-SiO₂^{6,7}. Models of the glass have been generated by quenching from the melt in classical molecular dynamics simulations and then annealed for few ps within ab-initio Car-Parrinello molecular dynamics⁸. The same method has been used by Ispas *et al.*⁹ to generate a theoretical model of sodium tetrasilicate glass $(\text{Na}_2\text{O})_{0.2}(\text{SiO}_2)_{0.8}$ (NS4) achieving good agreement with experiments both in the structural and electronic properties. Ispas *et al.*⁹ used a modified BKS-potential¹⁰ extended

to sodium silicates by Horbach *et al.*¹¹. Conversely, we have adopted the empirical potential developed by Oviedo *et al.*¹² which is an extension to sodium silicate glass of the forcefield introduced by Vashista *et al.*¹³ for pure amorphous silica. It consists of a short-range two-body interaction, long-range coulomb interactions, and a three-body term which enforces the directionality of the Si-O covalent bond. The Na-Si, Na-O and Na-Na interactions have been modeled by Oviedo *et al.*¹² by coulomb interactions plus a repulsive short-range term. The effective charges of the coulombic potential are: 1.0 for Na, 1.6 for Si, and -0.971 for oxygen which enforces charge neutrality in NS3 (note that there is a misprint in the oxygen charges in table I of ref.¹²). A model of liquid NS3 has been prepared by inserting 7 Na₂O and 21 SiO₂ units in a cubic box ($a=10.531$ Å) at the experimental density of glassy NS3 (2.427 g/cm³). The system is equilibrated at 6800 K, cooled to 3800 K in 50 ps and then equilibrated at the final temperature for 5 ns. The sample is then quenched at room temperature in 5 ns (quenching rate of $7 \cdot 10^{11}$ K/s) and equilibrated at 300 K for 50 ps. This model has then been annealed at 600 K in Car-Parrinello simulations for 1.3 ps and then quenched at 300 K in 0.15 ps. Structural properties have been averaged over a NVE run at room temperature, 1.1 ps long. The ab-initio simulations are based on density functional theory in the local density approximation (LDA)¹⁴ as implemented in the code CPMD⁸. Norm-conserving pseudopotential for Si and Na have been used. Non linear core corrections are included in Na pseudopotential¹⁵. An ultrasoft pseudopotential¹⁶ has been used for oxygen. Kohn-Sham (KS) orbitals are expanded in plane-waves up to a kinetic cutoff of 27 Ry. Integration of the BZ has been restricted to the Γ point. To study the dielectric properties, the structures generated by Car-Parrinello simulations have been then optimized with norm-conserving pseudopotentials and a larger cutoff of 70 Ry. We have computed the dielectric and photoelastic tensors within density functional perturbation theory DFPT¹⁷, as implemented in the code PWSCF and PHONONS¹⁸. The photoelastic tensor is defined by

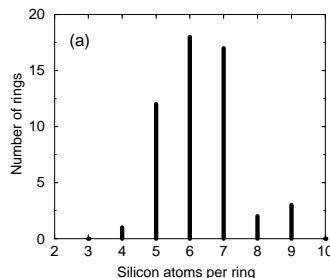
$$\Delta \varepsilon_{ij}^{-1} = p_{ijkl} \eta_{kl} \quad (1)$$

where ε_{ij} are the components of the optical dielectric tensor, η_{kl} is the strain tensor. Only the electronic contribution is included in ε_{ij} , also indicated as ε^∞ . Experimentally, it corresponds to the dielectric response measured for frequencies of the applied field much higher than lattice vibrational frequencies, but lower than the frequencies of the electronic transitions. The photoelastic coefficients have been calculated by finite differences from the dielectric tensor of systems with strains from -1 % to +1 %. The components of the photoelastic tensor will be expressed hereafter in the compressed Voigt notation.

The exchange-correlation functionals available in literature (LDA and generalized gradient approximation (GGA)) usually underestimate the electronic band gap and overestimate the electronic dielectric tensor up to 10-15 %¹⁹. This discrepancy can be corrected semi-empirically by applying a self-energy correction, also referred to as a scissor correction, which consists of a rigid shift of the conduction bands with respect to the valence bands²⁰. This procedure has been used successfully to reproduce the photoelasticity of Si²¹, GaAs²² and quartz¹⁹. However, as shown in our previous work⁶, it turns out that even within simple LDA, the error in the photoelastic coefficients for several polymorphs of silica is smaller than what expected on the basis of the error in the dielectric constant itself. The scissor correction has thus been neglected in the calculation on NS3 reported here.

III. STRUCTURAL PROPERTIES

As pointed out in previous works^{12,9,11}, the insertion of sodium modifies the topology of the network by the formation of non-bridging oxygens (NBO). The number of NBO coincides roughly (and in our small cell, exactly) with the number of Na atoms. All silicon atoms in our model are 4-fold coordinated and bonded at most with one NBO. The presence of NBO drastically reduces the number of medium sized rings (5-8 Si atoms per ring) which are usually predominant in the ring-size distribution of pure silica (Fig. 1).



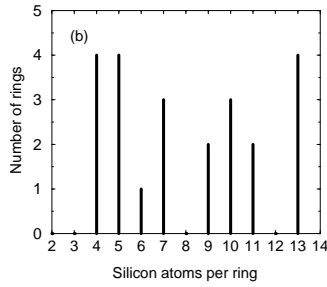


FIG. 1. The ring size distribution of (a) a model of pure α - SiO_2 ⁶ and of (b) the NS3 model after CPMD annealing.

The structural properties of the final ab-initio model of NS3 are compared to those of the classical model (before ab-initio annealing) in Figs. 2, 3 and 4. Pair correlation functions ($g(r)$) and radial coordination numbers are shown in Fig. 2. The average Si-O bond for NBO is slightly shorter than for bridging oxygen ions (BO) as shown in Fig. 5 which report $g_{\text{SiO}}(r)$ resolved for BO and NBO.

The ab-initio annealing produces a slight broadening of the pair correlation and angle distribution functions (ADF, Fig. 4). In fact, the three-body term in the classical potential assigns a tetrahedral geometry too stiff with respect to the ab-initio results. The O-Si-O ADF is still centered around the tetrahedral angle (109.5°), while the Si-O-Si ADF is centered at 139.3° , which is smaller than the average Si-O-Si angle in pure silica. Furthermore, in contrast with the classical models of pure silica generated with the BKS potential (cfr. ref.^{7,9,6}) no shift in the maximum of the $g(r)$ (SiO, OO and SiSi) is observed upon ab-initio annealing. In fact, the Vashista potential is fitted directly on the experimental $g(r)$ of amorphous silica and the agreement with ab-initio bondlengths is better than for the BKS potential. However, the ab-initio annealing shifts outwards the peak of the Na-O correlation function (from 2.4 to 2.5 Å). By separating the contribution of NBO and BO to the pair correlation functions (Fig. 3) we can see that the Na atoms are closer to NBO than to BO. On average, a NBO is coordinated with 2.9 Na ions and a BO with 1.3 Na ions. On the other hand, a Na ion is on average coordinated with about 2.9 NBO and 3.35 BO (cfr. Fig. 2).

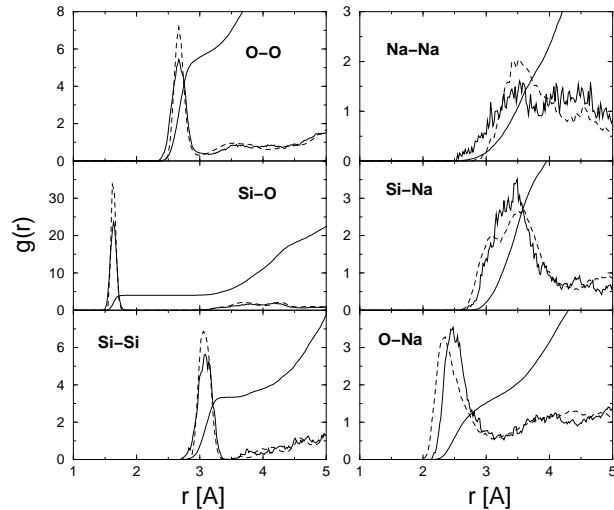


FIG. 2. Pair correlation functions of the NS3 model. Bold solid and dashed lines correspond to ab-initio and classical MD simulations, respectively. The thin solid line is the ab-initio radial coordination number.

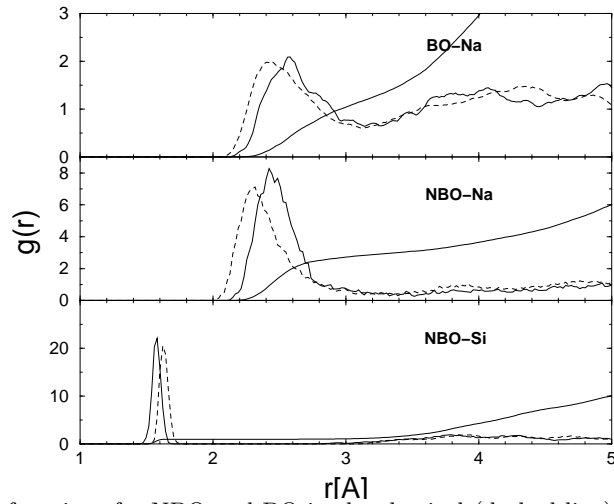


FIG. 3. Partial pair correlation functions for NBO and BO in the classical (dashed line) and ab-initio (bold line) models of NS3.

Looking at the Na-Na pair correlation function it is worth noting that the broad peak at 3.5 Å present in the classical MD model, disappears in the CPMD simulation. Thus, sodium does not tend to segregate or to form clusters, but it is homogeneously distributed in the network.

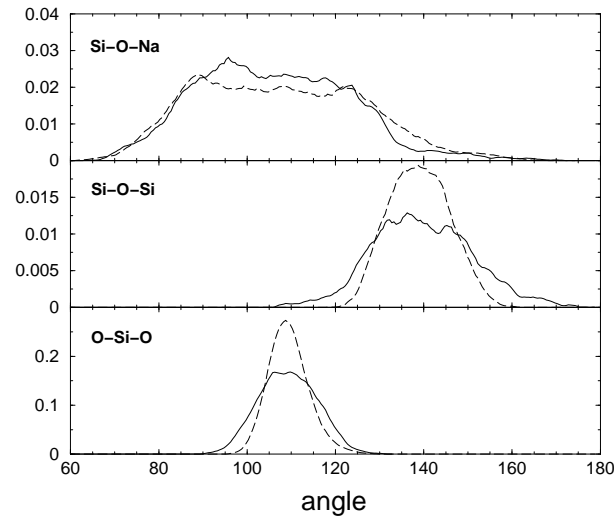


FIG. 4. Angular distribution functions. Bold solid and dashed lines correspond to ab-initio and classical MD simulations, respectively.

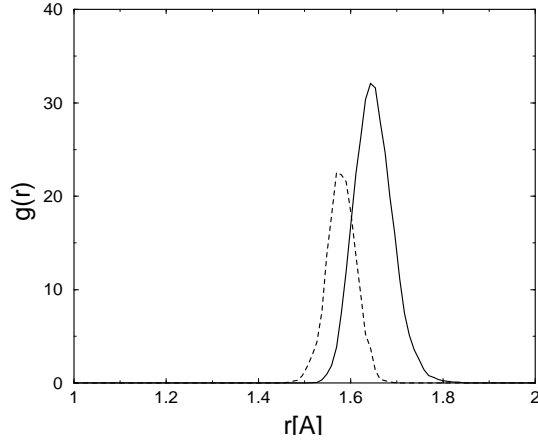


FIG. 5. Silicon-oxygen pair correlation function for NBO (dashed line) and BO (solid line) of the ab-initio model of NS3.

Our results on the structural properties of NS3 are close to those obtained by Ispas et al⁹ for a model of NS4 within a similar theoretical framework.

After the ab-initio annealing performed with the softer Vanderbilt pseudopotentials, the final structure has been further optimized with norm-conserving pseudopotentials (for the calculations of the dielectric properties). The cell geometry has been optimized at fixed volume allowing orthorhombic distortions of the initially cubic supercell such as to produce a diagonal stress tensor. The residual anisotropy in the stress (σ) for the optimized ratios of cell edges $b/a = 1.04$ and $c/a = 1$ is

$$\sigma = \begin{pmatrix} -502.8 & -10.9 & 4.03 \\ -10.9 & -495.1 & -18.6 \\ 4.03 & -18.6 & -503.1 \end{pmatrix} \text{ kbar} \quad (2)$$

The large negative stress in eq. 2 is due to the so-called Pulay stress. The b/a and c/a ratios obtained in this way at the experimental equilibrium density have been held fixed and the volume varied to generate the equation of state reported in Fig. 6.

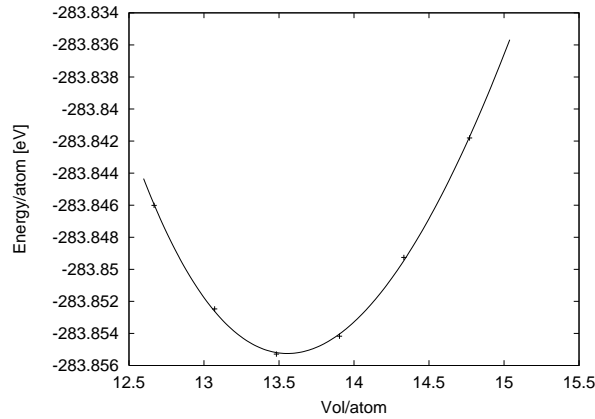


FIG. 6. Ab-initio equation of state of the NS3 model.

The calculated $E(V)$ points have been corrected for the discontinuities due to the incomplete basis set following the prescription given in ref.²³ and then fitted by a Murnaghan function²⁴. The resulting equilibrium density (ρ_{eq}), bulk modulus (B) and derivative of the bulk modulus with respect to pressure (B') are $\rho_{eq} = 2.468 \text{ g/cm}^3$ (exp. 2.427 g/cm^3), $B = 44.1 \text{ GPa}$, $B' = 1.6$. The insertion of Na produces a marginal softening of B with respect to pure silica⁶. In fact in our previous work⁶ on a model of a-SiO₂ of similar size (81 atoms) we obtained in our previous work⁶ we have obtained $\rho_{eq} = 2.31 \text{ g/cm}^3$, $B = 46.2 \text{ GPa}$, $B' = -6.28$. The value of B' , negative in pure silica, turns to positive in NS3, which means that the structural response to compression is different in silica and in NS3. Na-O interaction is probably responsible for the change in B' .

The response to strain (η_{22}, η_{33}) of some average structural parameters of NS3 and of a-SiO₂ (81-atoms supercell) are compared in table I. The change in the SiOSi angles upon strain is substantially smaller in NS3 than in pure

a-SiO₂, nevertheless the response of the Na-O distances to strain is rather relevant, if compared to the average Si-O distance changes, both in pure silica and in NS3.

TABLE I. The derivatives of the SiO and NaO bond-lengths, SiOSi angles and Si-Si nearest neighbors vector distances with respect to strains η_{22} and η_{33} in the models of NS3 and a-SiO₂⁶. $P_i(\text{Si-Si})$ denotes the projection of the average Si-Si vector distance on the i -th axis. NBO and BO indicate non-bridging and bridging oxygen atoms, respectively.

	NS3		SiO ₂	
	$\partial/\partial\eta_{22}$	$\partial/\partial\eta_{33}$	$\partial/\partial\eta_{22}$	$\partial/\partial\eta_{33}$
Si - O	0.145	0.125	0.154	0.157
Si- $\widehat{\text{O}}$ -Si	49.7	39.5	69.1	73.4
$P_x(\text{Si-Si})$	-0.218	-0.290	-0.037	-0.122
$P_y(\text{Si-Si})$	1.451	-0.131	1.553	-0.049
$P_z(\text{Si-Si})$	-0.026	1.303	-0.067	1.490
Na - BO	0.790	0.676	-	-
Na - NBO	0.479	0.280	-	-

IV. DIELECTRIC AND PHOTOELASTIC PROPERTIES

The dielectric tensor of the NS3 model optimized at its equilibrium density is:

$$\varepsilon = \begin{pmatrix} 2.449 & 0.008 & -0.006 \\ 0.008 & 2.438 & 0.031 \\ -0.006 & 0.031 & 2.474 \end{pmatrix}, \quad (3)$$

The average theoretical dielectric constant of NS3 and of pure silica (cfr. Ref.[6]) are compared to experimental data in table .

TABLE II. Theoretical and experimental dielectric constant of NS3 and pure a-SiO₂. ^a Ref.[6] .

	DFPT	exp. ⁴
NS3	2.454	2.236
a-SiO ₂	2.292 ^a	2.125

The increase of ε due to sodium insertion is quantitatively reproduced by our calculations. The computation of the photoelastic tensor has been performed by finite differences of the dielectric tensor by applying strains of $\pm 1\%$.

Results on the photoelastic coefficients are compared with experiments⁴ in table III. The p_{11} and p_{12} coefficients have been obtained by averaging over different components which should be equal in a homogeneous model, i.e. $p_{11} = (p_{33} + p_{22})/2$ and $p_{12} = (p_{12} + p_{13} + p_{23} + p_{32})/4$. The agreement with experimental data is of the same quality as for pure a-SiO₂. In particular, the calculation reproduces quantitatively the change in photoelastic coefficients observed experimentally upon insertion of Na, namely a large decrease of the off-diagonal p_{12} and a smaller increase of p_{11} .

TABLE III. Ab-initio photoelastic coefficients of the NS3 model compared with experimental data, with photoelastic coefficients of pure silica computed by DFPT and with measured ones.

	NS3		a-SiO ₂	
	This work	exp. ⁴	DFPT ⁶	exp. ⁴
p_{11}	0.097	0.134	0.057	0.125
p_{12}	0.167	0.214	0.220	0.27
p_{44}	-0.044	-0.040	-0.074	-0.073

V. PHENOMENOLOGICAL MODEL OF PHOTOELASTICITY

A. Pure silica glass

In a previous work⁶, we have developed a phenomenological model of the dielectric properties of silica based on ab-initio data. The main features of the model are briefly outlined here. Its extension to NS3 is described in the next section. In ref.⁶ we have assumed that the dielectric response of silica polymorphs could be embodied in an ionic polarizability tensor of the oxygen ions, whose value is assumed to depend on the Si \dot{O} Si angle only. The dielectric susceptibility $\underline{\underline{\chi}}$ ($\underline{\underline{\epsilon}} = 1 + 4\pi\underline{\underline{\chi}}$) can be obtained from a site dependent oxygen polarizability, $\underline{\underline{\alpha}}_i$, as

$$\underline{\underline{\chi}} = \frac{1}{V} \sum_{i,j}^N \underline{\underline{\alpha}}_i (\underline{\underline{I}} - \underline{\underline{B}})_{ij}^{-1}, \quad (4)$$

where V is the volume of the unit cell containing N oxygen ions and $\underline{\underline{B}}$ is a $3N \times 3N$ matrix consisting of 3×3 blocks $\underline{\underline{B}}_{ik}$ defined as

$$\underline{\underline{B}}_{ik} = \left(\frac{4\pi}{V} - \sum_{\vec{R}} \underline{\underline{T}}_{ik}^{\vec{R}} \right) \underline{\underline{\alpha}}_k \quad (5)$$

and

$$\underline{\underline{T}}_{ik}^{\vec{R}} = \nabla_i \nabla_k \left(\frac{1}{r_{ik}} \right) = \frac{1}{r_{ik}^3} \left[1 - 3 \frac{\vec{r}_{ik} \vec{r}_{ik}}{r_{ik}^2} \right], \quad (6)$$

where \vec{R} are Bravais lattice vectors defined by the shape of the supercell for models of glasses or by the unit cell for crystalline phases. r_{ik} is the distance between sites i and k in cells separated by \vec{R} (see Ref.⁶ for details).

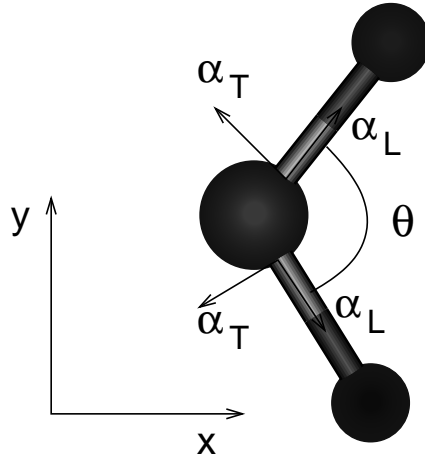


FIG. 7. Sketch of the Si-O-Si unit and of the bond contributions to polarizability.

The polarizability of the oxygen ions is a function of the SiOSi angle θ and can be expressed in terms of the polarizability of the SiO bonds as (cfr. ref.⁶)

$$\underline{\underline{\alpha}} = \begin{pmatrix} c(\theta) + \gamma \cos^2(\theta/2) & 0 & 0 \\ 0 & c(\theta) + \gamma \sin^2(\theta/2) & 0 \\ 0 & 0 & \alpha_{T'}(\theta) \end{pmatrix} \quad (7)$$

with $c = 2(\alpha_L + \alpha_T + \alpha_{T'})/3$, $\gamma = \alpha_L - \alpha_T$ and α_L , α_T and $\alpha_{T'}$ are the longitudinal and the two transversal polarizabilities of the Si-O bond in Fig. 7, respectively. The contribution of each polarizable SiOSi unit to the dielectric susceptibility is

$$\underline{\underline{\alpha}}_i = \underline{\underline{R}}_i^T \underline{\underline{\alpha}}(\theta) \underline{\underline{R}}_i \quad (8)$$

where $\underline{\underline{R}}_i$ is the rotation matrix that operates the transformation from the local reference system represented in figure 7 to the absolute reference system of the solid, in which the i -th Si-O-Si unit is embedded. The parameter γ has been assumed independent on θ and set equal to the value obtained from the fitting of the ab-initio Raman spectrum of α -quartz in ref.²⁵ ($\gamma = 9.86$ a.u.). As discussed in our previous work⁶, the functions $c(\theta)$ and $\alpha_{T'}(\theta)$ have been fitted on the dielectric properties of α -cristobalite at different densities. The results reported are shown in Fig. 8.

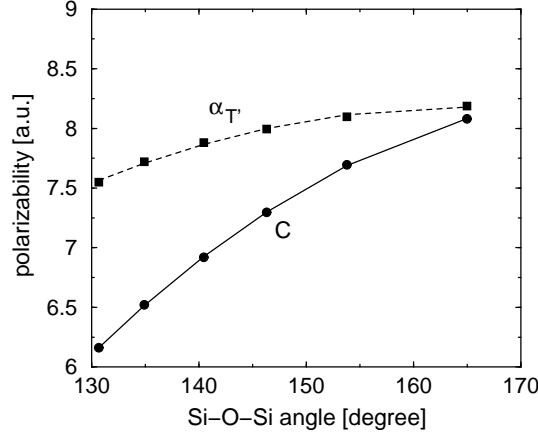


FIG. 8. The functions $c(\theta)$ (solid line and circles) and $\alpha_{T'}(\theta)$ (dashed line and squares), which assign the oxygen polarizability (see text). The data are the result of the fitting on the dielectric tensor of α -cristobalite at different densities.

This model allows the calculation of the photoelastic tensor given by the derivative of the dielectric susceptibility tensor χ (eq. 4) with respect to the strain tensor $\eta_{\lambda\mu}$ as

$$\begin{aligned} \frac{\partial \underline{\underline{\chi}}}{\partial \eta_{\lambda\mu}} = & -\underline{\underline{\chi}} \delta_{\lambda\mu} + \frac{1}{V} \sum_i^N \left(\left[\underline{\underline{R}}_i^T \frac{\partial \underline{\underline{\alpha}}}{\partial \eta_{\lambda\mu}} \underline{\underline{R}}_i \right] \underline{\underline{A}} + \right. \\ & \left. + \left[\underline{\underline{R}}_i^T \underline{\underline{\alpha}} \underline{\underline{R}}_i \right] \frac{\partial \underline{\underline{A}}}{\partial \eta_{\lambda\mu}} + \left[\frac{\partial \underline{\underline{R}}_i^T}{\partial \eta_{\lambda\mu}} \underline{\underline{\alpha}} \underline{\underline{R}}_i + \underline{\underline{R}}_i^T \underline{\underline{\alpha}} \frac{\partial \underline{\underline{R}}_i}{\partial \eta_{\lambda\mu}} \right] \underline{\underline{A}} \right) \end{aligned} \quad (9)$$

where the matrix $\underline{\underline{A}}$ is defined as $\underline{\underline{A}} = (\underline{\underline{I}} - \underline{\underline{B}})^{-1}$ (see eq. 4), and the arguments in square brackets indicate $3 \times 3N$ matrices. The change of the oxygen polarizability with strain can be expressed in terms of $\partial c(\theta)/\partial \theta$ and $\partial \alpha_{T'}(\theta)/\partial \theta$ deduced from Fig. 8. All the other derivatives can be obtained by finite differences. The phenomenological model outlined above has been shown to reproduce satisfactorily the dielectric and photoelastic tensors of several silica polyphorms (quartz, α -cristobalite, β -cristobalite, a-SiO₂) at normal conditions and at high density⁶.

B. Extension to sodium silicates

We can now make use of this phenomenological model for pure a-SiO₂ to identify which term in Eq. 9 is mostly affected by the presence of sodium. As shown in Ref.⁴ the change in ε and in the density alone within a simple Lorenz-Lorentz model (cfr. section II) can not account for the change in the photoelastic coefficients measured experimentally upon Na insertion. This is inferred by comparing the quantity $\rho \partial \varepsilon / \partial \rho$ measured experimentally ($(\rho \partial \varepsilon / \partial \rho)_{obs} = \varepsilon^2(p_{11} + 2p_{12})/3$) with the result of the Lorenz-Lorentz model

$$\left(\rho \frac{\partial \varepsilon}{\partial \rho} \right)_{LL} = \frac{(\varepsilon - 1)(\varepsilon + 2)}{3} \quad (10)$$

For pure a-SiO₂, $(\rho \partial \varepsilon / \partial \rho)_{obs} = 1.003$ and $(\rho \partial \varepsilon / \partial \rho)_{LL} = 1.547$, while for NS3 $(\rho \partial \varepsilon / \partial \rho)_{obs} = 0.937$ and $(\rho \partial \varepsilon / \partial \rho)_{LL} = 1.746$. Thus, the Lorenz-Lorentz model predicts an increase in the photoelastic response with Na content

which is in contrast with the experimental observation. An increase in the dependence of the molecular polarizability upon strain ($\partial\alpha/\partial\eta$ in Eq. 9), neglected in the Lorentz-Lorenz model, is required to account for a decrease in p_{12} . By still keeping valid the phenomenological model of pure silica, we may argue that the quantity $\partial\alpha/\partial\eta$ may change with Na content because of different possible effects: i) a change of the elastic response of the system (via $\partial\theta/\partial\eta$), ii) a change in the functional dependence of the BO polarizability on the SiOSi angle (cfr. Fig. 8), iii) other structural parameters which become relevant with the presence of Na (such as the NaO interaction for instance) control the response to strain of the polarizability of BO, iv) the NBO contribute to a term in $\partial\alpha/\partial\eta$. In ref.⁵ Lines has conjectured that the decrease in the photoelastic coefficients in NS glasses might be due to an increased modulation of the SiO bond length by strain, i.e. the Na ions would simply modify the mechanical response of the glass. However, we can recognize that this conjecture is not supported by the results in table I. In fact, the modulation of the SiO bond length upon even decreases in NS3 with respect to pure silica (cfr. table I). In order to clarify these issues, we have extended the phenomenological model for pure silica by considering different polarizabilities for NBO and BO. We have introduced an additional parameter, α_{NBO} , which describes a spherical polarizability of NBO ions. We have further assumed that α_{NBO} may depend on the local electric field (E_{loc}) produced by the Na^+ ions. The modulation of the Na-NBO distances upon strain would thus contribute to $\partial\alpha/\partial\eta$ in the photoelastic tensor via a term of the form

$$\frac{\partial\alpha_{NBO}}{\partial\eta} = \frac{\partial\alpha_{NBO}}{\partial E_{loc}} \frac{\partial E_{loc}}{\partial\eta}. \quad (11)$$

We have fitted the parameter $\partial\alpha_{NBO}/\partial E_{loc}$, which describes the response of the NBO polarizability to the local field of Na^+ on the photoelastic coefficients of a sodium silicate crystal: the natrosilite $\text{Na}_2\text{Si}_2\text{O}_5$ ²⁶.

1. Natrosilite

Natrosilite is a layered material with NBO nearly aligned along the c -axis, perpendicular to the siloxane layers (Fig. 1). Details on the structure of natrosilite are given in the appendix.

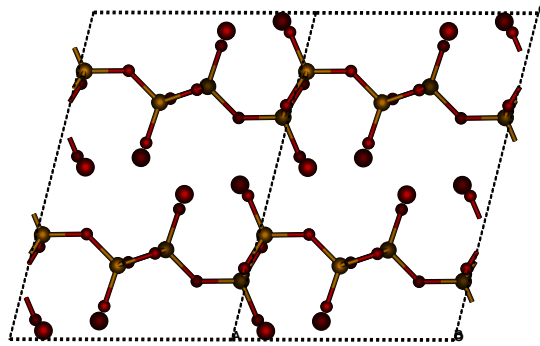


FIG. 9. Side view of the natrosilite crystal. Large (small) dark grey spheres are Na (O) ions. Light grey spheres are Si ions.

By changing the length of the c axis with the other lattice parameters (a , b and β , see appendix) fixed, the SiOSi angles of BO do not change while there is a large change of the Na-NBO distances. We have thus assumed that the change in the dielectric constant of natrosilite upon the η_3 strain would be entirely due to the change of α_{NBO} which would obviously lead to an overestimation of $\partial\alpha_{NBO}/\partial\eta$. We have thus considered a model for the dielectric response of natrosilite in which the BO have the same polarizability as in pure silica (cfr. section Va) and the two additional parameters of NBO, α_{NBO} and $\partial\alpha_{NBO}/\partial\eta_3$, have been fitted on the ab-initio photoelastic coefficient of natrosilite p_{13} , p_{23} , and p_{33} . We obtain $\alpha_{NBO} = 14.6$ a.u. and $\partial\alpha_{NBO}/\partial\eta_3 = 20.5$ a.u. From Eq. 11

$$\frac{\partial\alpha_{NBO}}{\partial\eta_3} = \frac{\partial\alpha_{NBO}}{\partial E_{loc}} \frac{\partial E_{loc}}{\partial\eta_3} = \frac{\partial\alpha_{NBO}}{\partial E_{loc}} N_{Na} \frac{\partial \langle r_{NaO}^{-2} \rangle}{\partial\eta_3} \quad (12)$$

where we have assumed

$$E_{loc} = N_{Na} \langle r_{NaO}^{-2} \rangle, \quad (13)$$

N_{Na} is the number of Na ions nearest neighbor to NBO and r_{NaO} is the Na-NBO distance. The average is over the nearest neighbor ions. In natrosilite $N_{Na}=4$ and $\langle r_{NaO}^{-2} \rangle = 0.177 \text{ \AA}^{-2}$ which finally yields $\partial\alpha_{NBO}/\partial E_{loc} = -29.3 \text{ a.u.}$. Table IV reports the ab-initio photoelastic coefficients of natrosilite and the results of the phenomenological model outlined above. The quantity $\partial\alpha_{NBO}/\partial E_{loc}$ is negative which means that by moving the Na ions further away from the NBO its polarizability increases. In fact, by decreasing the local electric field on NBO its charge would become more diffuse and thus more polarizable. The ab-initio photoelastic tensor has been computed by finite differences from the dielectric tensor calculated within DFPT with the codes PWSCF and PHONONS as described in section II. The calculations have been performed at the experimental equilibrium volume (see appendix).

TABLE IV. Average values of the phenomenological polarizability of BO and NBO ions and photoelastic coefficients of natrosilite computed ab-initio (DFPT) and with the phenomenological model described in the text.

	Model	DFPT
$\overline{\alpha_{BO}}$	10.6	-
$\overline{\alpha_{NBO}}$	14.62	-
ε_{11}	2.454	2.412
ε_{22}	2.467	2.443
ε_{33}	2.282	2.361
p_{13}	0.140	0.131
p_{23}	0.143	0.138
p_{33}	0.087	0.104

2. NS3 glass

In the development of a model for photoelasticity in NS3, we have used the value of $\partial\alpha_{NBO}/\partial E_{loc}$ obtained from the fitting on natrosilite described in the previous section. The differences in the environment of NBO and in the structural response to strain of NS3 with respect to natrosilite is accounted for by the term $\partial E_{loc}/\partial\eta$ in Eq. 12. In our model of NS3, $N_{Na}=2.8$ and $\langle r_{NaO}^{-2} \rangle = 0.166 \text{ \AA}^{-2}$ (cfr. section III). To extend the phenomenological model to NS3, we have considered two extreme cases as described below.

a) In the first case (model A) we have assumed that the polarizability of BO ions (α_{BO}) is the same as in pure a-SiO₂ and assigned by the curves in Fig. 8. The polarizability of NBO, α_{NBO} , is then assigned by fitting the ab-initio dielectric constant of NS3 within our extended phenomenological model. The contribution from $\partial\alpha_{NBO}/\partial E_{loc}$, fitted on natrosilite, is added. The results are reported in table V. The fitting yields $\alpha_{NBO} = 17.0 \text{ a.u.}$, a value larger than α_{NBO} in natrosilite (cfr. table IV), as we would have expected by considering that $\partial\alpha_{NBO}/\partial E_{loc}$ is negative and E_{loc} is lower in NS3 with respect to natrosilite (cfr. Eq. 13). If we change by 20 % the value of α_{NBO} (a change comparable with the difference in α_{NBO} between natrosilite and NS3) in the fitting procedure on natrosilite, one obtains a value for $\partial\alpha_{NBO}/\partial E_{loc}$ with a similar change of 20 % with respect to the data in table IV. However, a change in $\partial\alpha_{NBO}/\partial E_{loc}$ of the order of 20 % does not affect the the results on the photoelastic coefficients of NS3 within the figures reported in table V.

b) In the second case (model B) α_{NBO} is set to zero and α_{BO} is still assigned by the function given in Fig. 8, but rescaled by a multiplicative factor in order to reproduce the dielectric constant of NS3. In this way we have also rescaled the term $\partial\alpha_{BO}/\partial\eta$ depending on the SiOSi angle. The increase of the polarizability of the BO upon Na insertion is supported by the comparison of the calculated Born effective charges for our models of NS3 and a-SiO₂ shown in Fig. 10. The presence of Na induces a nearly uniform increase of the Born effective charges of BO ions. The valence electrons of the ionized Na atoms are thus transferred to both NBO and BO ions. A larger charge on the BO ions implies a larger polarizability.

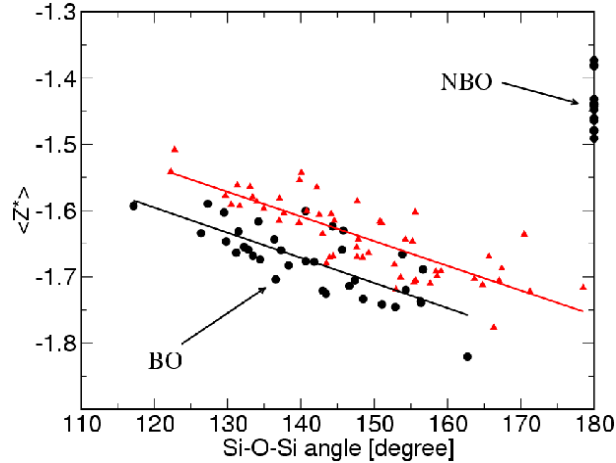


FIG. 10. Dependence of the Born effective charges of oxygen atoms as a function of the Si-O-Si angle in the models of NS3 (black circles) and a-SiO₂ (red triangles, from ref.⁶). BO and NBO indicate bridging and non-bridging oxygen ions, respectively.

In this model the contribution from NBO is added as well with the same parameter $\partial\alpha_{NBO}/\partial E_{loc}$ fitted on natrosilite and used in model A. The results are reported in table V.

TABLE V. Average values of the phenomenological polarizability of BO and NBO ions and photoelastic coefficients according to the two models (A and B) described in the text. The ab-initio (DFPT) photoelastic coefficients of NS3 and pure a-SiO₂ (ref.⁶) are also reported. Results including and neglecting the term $\partial\alpha_{NBO}/\partial E_{loc}$ (in a.u., see text) are both reported.

	NS3					a-SiO ₂	
	Model A		Model B	DFPT		Model	DFPT
$\overline{\alpha_{BO}}$	10.6	10.6	17.8	17.8	-	10.6	-
$\overline{\alpha_{NBO}}$	17.0	17.0	0	0	-	-	-
$\partial\alpha_{NBO}/\partial E_{loc}$	0	-29.33	0	-29.33	-	-	-
p_{21}	0.25	0.24	0.24	0.23	0.167	0.227	0.220
p_{22}	0.18	0.17	0.14	0.13	0.072	0.097	0.057

Both models A and B largely overestimate the photoelastic coefficients in NS3 with respect to pure a-SiO₂.

As mentioned before the value used for $\partial\alpha_{NBO}/\partial E_{loc}$ overestimates the real contribution of NBO to $\partial\alpha/\partial\eta$ in NS3. Yet, although overestimated, NBO gives a very small contribution to the photoelastic tensor. Even within model B where the contribution of BO is also rescaled by a factor 1.7 by still keeping α_{BO} dependent on the SiOSi angle only, the model photoelastic coefficients are sizably larger than the ab-initio data. The failure of these models suggests that either the shape of the functions in Fig. 8 changes upon Na insertion and/or other structural parameters, in addition to the SiOSi angle, influence the polarizability of BO ions.

VI. CONCLUSIONS

Photoelasticity in a model of sodium silicate glass (NS3) has been studied within density functional perturbation theory. The NS3 model is generated by quenching from the melt in combined classical and Car-Parrinello molecular dynamics simulations.

The calculated photoelastic coefficients are in good agreement with experimental data and further confirm the reliability of DFPT already assessed for pure silica polymorphs in our previous work⁶. In particular, the calculation reproduces quantitatively the decrease of the photoelastic response induced by the insertion of Na, as measured experimentally⁴. Aiming at identifying the microscopic mechanisms thorough which sodium modifies the photoelastic response of the glass, we have extended to NS3 a phenomenological model of photoelasticity developed for pure silica in our previous work⁶. It comes out that the contribution of NBO to the photoelastic tensor (via a modulation of the NBO polarizability with strain) is not large enough to explain the decrease of the photoelastic coefficient of NS3 with respect to that of pure a-SiO₂. Moreover, although a charge transfer takes place from the ionized Na ions to the BO ions, a simple increase of the polarizability of BO is not sufficient to explain the change in the photoelastic response by keeping the SiOSi angle as the only structural parameter which modules the polarizability upon strain as in pure a-SiO₂. The modulation upon strain of other structural parameters should be called for. In order to quantify these latter effects, a more detailed modeling of the must be devised, requiring the fitting of the dielectric properties over a large database of sodium silicate crystals.

* present address: Computational Science, Department of Chemistry and Applied Biosciences, ETH Zurich, USI Campus, Via Giuseppe Buffi 13, CH-6900 Lugano, Switzerland.

ACKNOWLEDGMENTS

D.D. acknowledges Pirelli Cavi e Sistemi S.p.a. for financial support.

APPENDIX A

Natrosilite, Na₂O(SiO₂)₂, is a phyllosilicate crystal with space group P21/c and 4 formula units per unit cell²⁶. We have optimized the internal structure at the experimental equilibrium lattice parameters $a=8.13$ Å, $b=4.85$ Å, $c=12.33$ Å and $\beta = 104.3$ ^{o26}. We have used the code PWSCF¹⁸ and 2x2x2 Monkhorst-Pack²⁷ mesh for Brillouin Zone integration. The experimental and theoretical positions (in crystallographic units) of the 9 independent atoms are reported in table VI

TABLE VI. Experimental²⁶ and theoretical positions (in crystallographic units) of the independent atoms of natrosilite.

	Exp.			DFT		
	x	y	z	x	y	z
Si	0.028	0.184	0.183	0.027	0.164	0.181
Si	0.403	0.295	0.277	0.402	0.304	0.276
Na	0.379	0.753	0.443	0.381	0.752	0.443
Na	0.137	0.225	0.473	0.143	0.210	0.475
O	0.029	0.859	0.215	0.026	0.832	0.216
O	0.454	0.620	0.267	0.445	0.637	0.262
O	0.226	0.246	0.181	0.225	0.242	0.179
O	0.391	0.232	0.401	0.388	0.243	0.400
O	0.093	0.755	0.436	0.093	0.721	0.439

-
- ¹ H. Limberger, P. Fonjallaz, R. Salathe, and F. Cochet, *Appl. Phys. Lett.* **68**, 3069 (1996).
- ² R. Schenker and W. Oldman, *J. Appl. Phys.* **82**, 1065 (1997).
- ³ J. Schroeder, in *Treatise on Materials Science and Technology*, Vol. 12, Edited by M. Tomozawa and R. H. Doremus (Academic Press, New York, 1977), p. 157.
- ⁴ J. Schroeder, *J. Non-Cryst. Solids* **40**, 549 (1980).
- ⁵ M. E. Lines, *J. Non-Cryst. Solids* **103**, 279 (1988).
- ⁶ D. Donadio, M. Bernasconi, and F. Tassone, *Phys. Rev. B* **68**, 134202 (2003).
- ⁷ M. Benoit, S. Ispas, P. Jund, and R. Jullien, *Eur. Phys. J. B* **13**, 631 (2000).
- ⁸ CPMD V3.5 Copyright IBM Corp 1990-2001 and Copyright MPI für Festkörperforschung Stuttgart 1997-2001 .
- ⁹ S. Ispas, M. Benoit, P. Jund, and R. Jullien, *Phys. Rev. B* **64**, 214206 (2001).
- ¹⁰ B. W. H. van Beest, G.J. Kramer, and R.A. van Santen, *Phys. Rev. Lett.* **64**, 1955 (1990).
- ¹¹ J. Horbach and W. Kob, *Phil. Mag. B* **79**, 1981 (1999).
- ¹² J. Oviedo and J. F. Sanz, *Phys. Rev. B* **58**, 9047 (1998).
- ¹³ P. Vashishta, R. K. Kalia, J. P. Rino, and I. Ebbsjo, *Phys. Rev. B* **41**, 12197 (1990).
- ¹⁴ J.P. Perdew and A. Zunger, *Phys. Rev. B* **23**, 5048 (1981).
- ¹⁵ S.G. Louie, S. Froyen, and M.L. Cohen, *Phys. Rev. B* **26**, 1738 (1982).
- ¹⁶ D. Vanderbilt, *Phys. Rev. B* **41**, 7892 (1990).
- ¹⁷ S. Baroni, S. de Gironcoli, A. dal Corso, and P. Giannozzi, *Rev. Mod. Phys.* **73**, 515 (2001).
- ¹⁸ S. Baroni, A. dal Corso, S. de Gironcoli, and P. Giannozzi, <http://www.pwscf.org> .
- ¹⁹ F. Detraux and X. Gonze, *Phys. Rev. B* **63**, 115118 (2001).
- ²⁰ Z. H. Levine and D. C. Allan, *Phys. Rev. B* **43**, 4187 (1991).
- ²¹ Z.H. Levine *et al.*, *Phys. Rev. B* **45**, 4131 (1992).
- ²² J.E. Raynolds, Z.H. Levine, and J.W. Wilkins, *Phys. Rev. B* **51**, 10477 (1995).
- ²³ G. Francis and M. Payne, *J. Phys. Condens. Matt.* **2**, 4395 (1990).
- ²⁴ D. Murnaghan, *Proc. Nat. Acad. Sci. USA* **30**, 224 (1944).
- ²⁵ P. Umari, A. Pasquarello, and A. Dal Corso, *Phys. Rev. B* **63**, 094305 (2001).
- ²⁶ A. Pant, *Acta Crystallographica B* **24**, 1077 (1968).
- ²⁷ H. J. Monkhorst and J. D. Pack, *Phys. Rev. B* **13**, 5188 (1976).